Cellulose (2019) 26:3271–3284
https://doi.org/10.1007/s10570-019-02270-x

ORIGINAL RESEARCH

Facile preparation of reactive hydrophobic cellulose nanofibril film for reducing water vapor permeability (WVP) in packaging applications

Wei Li · Shuangfei Wang · Wei Wang · Chengrong Qin · Min Wu

Received: 7 June 2018 / Accepted: 17 January 2019 / Published online: 31 January 2019

Abstract Due to energy crisis and environmental pollution, biopolymer-based packaging materials have been extensively investigated. Cellulose nanofibrils (CNFs), due to their good oxygen barrier performance and excellent mechanical as well as film-forming properties, have emerged as interesting packaging materials. However, the problem of the resulting films is the highly hygroscopic character of the cellulose fibers themselves, which would further lead to a decrease of the films' mechanical and barrier properties. Herein, a facile preparation of hydrophobic CNF films was carried out by the attachment of 10-undecylenoyl chloride onto CNFs followed by vacuum filtration. The modified CNFs became thicker and rougher compared with the pristine CNFs and were easy to disperse in ethanol. The resulting CNF film showed a higher surface roughness and a tensile strength of (47 ± 4) MPa. Additionally, the modified CNF film was hydrophobic, leading to an obvious barrier improvement with the WVP value decreasing by 62.4% in comparison to the pristine CNF film. Since this hydrophobic CNF film is easy to prepare with a good vapor barrier property, it should be promising for packaging applications. Furthermore, the generated CNF film demonstrated good reactivity with thiol groups, which can be applied for further functionalization to enrich their application fields.

W. Li · S. Wang · W. Wang · C. Qin · M. Wu (✉)
College of Light Industry and Food Engineering, Guangxi University, Nanning 530004, China
e-mail: wumin@gxu.edu.cn

W. Li
State Key Laboratory of Pulp and Paper Engineering, South China University of Technology, Guangzhou 510640, China

W. Li · S. Wang · W. Wang · C. Qin · M. Wu
Guangxi Key Laboratory of Clean Pulp and Papermaking and Pollution Control, Nanning 530004, China

Graphical abstract

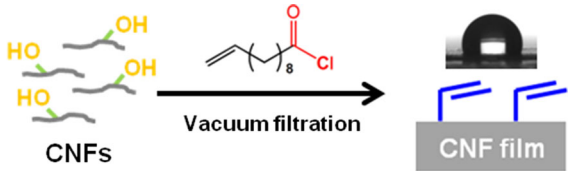

Keywords Cellulose nanofibrils (CNFs) · Acylation · Hydrophobicity · Dispersion properties · Water vapor permeability (WVP)

Introduction

Global warming as well as environmental pollution have become the main problems in the world. An important related field is packaging films, which mainly rely on petroleum-derived synthetic plastics. In order to alleviate such issues, biopolymer-based packaging materials derived from renewable forest resources have been extensively investigated (Azeredo et al. 2017; Rajinipriya et al. 2018; Song et al. 2014).

It is known that cellulose materials are the most abundant biomass materials in nature. Cellulose fibers, in the form of paper and paperboard, have been used in packaging for a wide range of food categories, such as dry foods, frozen or liquid foods, and even fresh foods (Spence et al. 2010). Recently, cellulose nanofibrils (CNFs) produced by a mechanical disintegration process of plant biomass have emerged as interesting packaging materials due to their good barrier (e.g. oxygen under dry conditions) and mechanical performance as well as excellent film-forming properties (Abdul Khalil et al. 2014; Ferrer et al. 2017; Le et al. 2016; Nechyporchuk et al. 2016).

Although the resulting CNF films have a great prospect in packaging materials, the main challenge of these films is associated with the very hygroscopic character of the cellulose fibers themselves. Thereby, the CNF films are considerably permeable when they are exposed to water or high relative humidity (RH) conditions. In this case, the interfibrillar hydrogen bonds are weakened or even partially cleaved by the intercalation of water molecules between cellulosic chains, resulting in the swelling of the films, which further leads to the decrease in the films' mechanical and barrier properties (Aulin et al. 2010; Benitez et al. 2013; Prakobna et al. 2015; Shimizu et al. 2016; Wang et al. 2018a, b).

In order to solve the above-mentioned problems, functionalization of CNFs with hydrophobic moieties could be a promising strategy (Song and Rojas 2013; Teisala et al. 2014), and various techniques have already been reported, e.g., impregnation of resins (Lu et al. 2016; Qing et al. 2015) or lignin (Rojo et al. 2015), coating with cationic surfactants (Shimizu et al. 2014) or waxes (Österberg et al. 2013), and chemical modification by silylation (Chinga-Carrasco et al. 2012), esterification (Sehaqui et al. 2014), acetylation (Jonoobi et al. 2010), amidation (Johnson et al. 2011) as well as polymer grafting (Stenstad et al. 2008).

Generally, the preparation of hydrophobic CNFs by a covalent attachment is preferred in order to obtain a homogeneous and robust structure under wet conditions as well as avoid the introduction of environmentally-unfriendly materials (Chinga-Carrasco et al. 2012). Acetylation is one of the first chemical reactions used for cellulose fibers and is still important and prevalent for hydrophobization (Cunha et al. 2014; Klemm et al. 1998). Tingaut et al. (2010) and Tomé et al. (2011) reinforced poly(lactic acid) (PLA) with acetylated CNFs and found that the moisture sorption/water uptake reduced in comparison to that of sample with unmodified CNFs. Previous research usually tends to focus on the moisture sorption of composites containing acetylated CNFs but seldom on that of the acetylated CNFs separately. Furthermore, there are few studies on the pure acetylated CNF films. Recently, Solala et al. (2018) prepared porous (~ 50%) nanofibrillated cellulose (NFC) films by vacuum filtration, solvent exchange with acetone and further hydrophobization with an epoxy modifier. The generated films were non-wettable by water but permeable to water vapor with a similar water vapor transport rate (WVTR) value to that of the unmodified NFC films. The authors ascribed this phenomenon to the porous structure of the resulting films, and concluded that water vapor transport was not influenced by the surface hydrophobization.

Their interesting research aroused us to investigate whether hydrophobization of CNFs before film formation and avoidance of solvent exchange after film formation would generate novel CNF films with decreased WVTR/WVP values. Herein, a facile

preparation of reactive hydrophobic CNF film was carried out by first attachment of 10-undecylenoyl chloride onto CNFs followed by film formation with vacuum filtration (as shown in Fig. 1). Unbleached pulps were chosen for the production of CNFs mainly due to their high yield, low environmental impact, low production cost, and the hydrophobicity as well as the high thermal stability of lignin (Ferrer et al. 2012; Nair & Yan 2015; Nair et al. 2017; Poletto et al. 2012; Rojo et al. 2015). The dispersion properties of the modified CNFs in water, a mixture of ethanol and water with a volume ratio of 1 to 1, and ethanol, were discussed. Subsequently, the chemical structure, morphology, thermal stability and mechanical properties of the generated CNF film were investigated followed by the studies of its wettability, water uptake and WVP performance and reactivity.

Experimental

Materials

Unbleached eucalyptus pulp obtained through chemical pulping was acquired from Yongkai Sugar and Paper Group (Guangxi, China). The contents of cellulose, hemicellulose and lignin in the pulp were 68.0%, 26.6% and 5.2%, respectively. The kappa number, brightness and viscosity of the pulp were 30.9, 39.8% ISO, and 1015 mL/g, respectively (Nie et al. 2018). 10-undecylenoyl chloride (98%) and ethylenediaminetetraacetic acid (EDTA, 99.5%) were bought from Shanghai Macklin Biochemical Co. Ltd. 3-mercaptopropionic acid, 2,2-dimethoxy-2-phenylacetophenone (DMPA), acetone, N,N-dimethylacetamide (DMAc), pyridine and ethanol were of analytical grade and purchased from Shanghai Aladdin Biochemical Technology Co. Ltd. All the chemicals were used as received.

Preparation of CNFs

Since the counter-ion form of the chosen unbleached eucalyptus pulp is mainly in the calcium form, a chelating treatment that was performed by washing with EDTA was first carried out to eliminate its effect. The pulp was then moisture equilibrated and the pulp consistency was kept at 2%. Finally, the pulp was defibered by disintegrator (3000 r/min, AG 04, Estanit, Germany) for 30–40 min and ground by a Superfine grinding mill (1500 rpm, Super Masscolloider MKZA 10-15JIV, Masuko Sangyo Co. Ltd, Japan) for 20 passes.

Acylation of CNFs

CNFs (1 g) were dispersed in water to obtain a CNF suspension with a concentration of 1.1%. The aqueous suspension was then solvent-exchanged with acetone by centrifuge (H1850, Xiangyi Centrifuge Instrument Co. Ltd., China) at 10619 $\times g$ (room temperature (RT), 10 min) for three times followed by solvent exchange with DMAc. The obtained solid was suspended into DMAc (100 mL). 10-undecylenoyl chloride with a molar ratio of 1.5 to that of CNFs was added into the above suspension. Note that, the

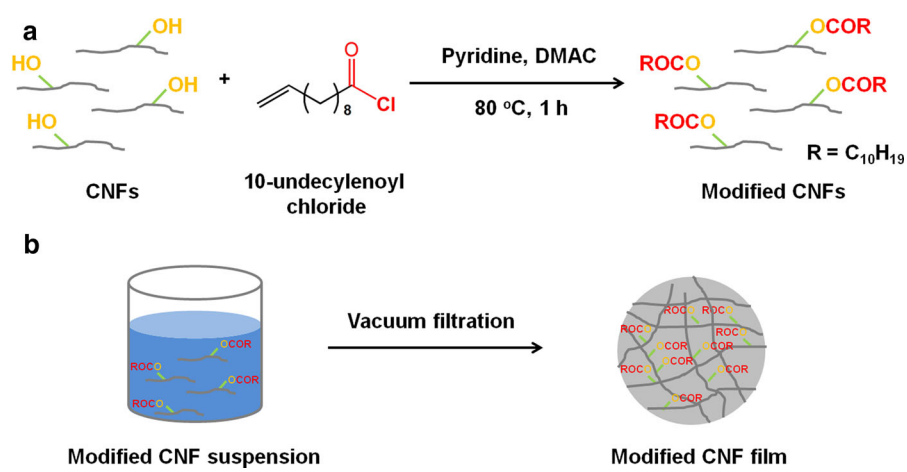

Fig. 1 Schematic illustration of the preparation of the modified CNFs (**a**) and the modified CNF film (**b**)

number of OH groups per gram of CNFs is approximately estimated with the hypothesis that the composition of CNFs is pure cellulose. In this case, it can be calculated as three times of the mole of CNFs that is roughly estimated as the quotient between the mass of CNFs and the molar weight of the glucose unit. This calculation method is also applied in the research by Solala et al. (2018) and Tingaut et al. (2010). Pyridine was added as catalyst with a molar ratio of 3 to that of 10-undecylenoyl chloride. The mixed suspension was reacted at 80 °C for 1 h. After reaction, the suspension was dropped into ethanol (100 mL) followed by centrifuge at 10619 $\times g$ (RT, 10 min). The obtained solid was dispersed into DMAc (80 mL) again and stirred for 3 h. The above suspension was then poured into ethanol (100 mL) and centrifuged under the same conditions. The process of dispersion in DMAc and pouring into ethanol was repeated for three times for purification. Finally, the obtained CNFs were dispersed in ethanol (150 mL) for further usage. The suspension of the modified CNFs in other solvents was prepared by solvent exchange.

Preparation of the pristine CNF film and the modified CNF film

CNF films were prepared by vacuum filtration. In brief, the modified CNFs ($\approx$ 0.18 g, dry weight) was dispersed in different solvents (200 mL), that is, ethanol, a mixture of ethanol and water with a volume ratio of 1 to 1, and water. The resulting suspension of CNFs was then filtrated by Buchner funnel with a piece of filter paper underneath and a piece of PTFE membrane (the pore size of 0.22 μm) on the top. The filtration time was approximately 10 min. The generated CNF film was dried between two pieces of filter paper at RT under pressure (7.64 kPa) followed by drying under vacuum at RT overnight and storage in the desiccator before further usage (named as the modified CNF film). Additionally, the pristine CNFs with the same amount were dispersed in water followed by vacuum filtration and drying in the same way. The resulting pristine CNF film was used as reference.

Reactivity study of the modified CNF film

In order to verify the possibility of further functionalization of the modified CNF film, the film (20 mm × 20 mm) was immersed into an ethanol solution of 3-mercaptopropionic acid (0.5 vol%, 5 mL) with DMPA (0.012 mol L^{-1}) as catalyst under UV illumination. After 10 min, the resulting film was thoroughly washed by ethanol and dried under vacuum at RT overnight as well as storage in the desiccator before further usage.

Characterization

Calculation of the degree of substitution

The contents of carbon, hydrogen and nitrogen were determined with Elemental Analyser Vario EL cube CHNSO from Elementar (Germany). The total degree of substitution (DS) of 10-undecylenoyl chloride was calculated according to the following equation (Vaca-Garcia et al. 2001):

$$DS = \frac{5.13766 - 11.5592 \times C\%}{0.996863 \times C\% - 0.856277 \times n + n \times C\%} \quad (1)$$

here, C% is the determined content of carbon and n is the number of carbon atom in the acyl substituent.

Morphology

The morphology of the pristine CNFs and the modified CNFs was investigated by transmission electron microscopy (TEM, Hitachi HT7700, Japan) operated at 100 kV. The CNF suspension in water (for the pristine CNFs) or ethanol (for the modified CNFs) was diluted to 0.008 wt% and stirred for 3 h. A drop of the CNF dispersion was carefully dropped onto a copper grid coated with carbon and allowed to dry at RT. The sample was then dyed with a drop of staining agent (3% phosphotungstic acid stain, pH 7.0). 20 min later, the excess liquid was removed with filter paper, and the sample was dried under ambient conditions. Finally, their diameter was analyzed by software (Nano Measurer 1.2.5). Meanwhile, the morphology of the generated pristine CNF film and the modified CNF film was measured by scanning electron microscopy (SEM) and atomic force microscopy (AFM). The SEM measurement was carried out in PHENOM F16502 scanning microscope (Netherland) operated at an acceleration voltage of 10 kV with gold-sputtered

samples. As for AFM imaging, the sample was scanned with a Nanoscope device (Hitachi 5100 N, Japan) in "multimode" mode in air using a commercial silicon tapping probe (SI-DF40P2, NanoWorld AG, Switzerland) with a resonance frequency of about 299 kHz. The average roughness (Ra) was measured from the AFM image by using the arithmetic average of absolute in the scanning area (5 μm × 5 μm).

Physical properties

The grammage of the pristine CNF film and the modified CNF film was obtained by weighing five pieces of films with known areas, and their thickness was measured by a digital micrometer (Buchel BV, The TMI Group of Companies, Holland) on at least five different spots. Based on the above two values, the average density of the films was finally calculated. Furthermore, according to the literature (Sehaqui et al. 2014), the porosity of the films was calculated from their density by taking 1500 kg m^{-3} as density for CNF (ρCNF) using the following equation:

$$Porosity = 1 - \frac{\rho}{\rho_{CNF}} \quad (2)$$

Chemical structure

The chemical structure of the pristine CNF film and the modified CNF film was identified by ATR FTIR spectroscopy (TENSOR II, Brook Technology, Germany). FTIR spectra were recorded in the region of 4000–400 cm^{-1}. 10 scans were accumulated with a resolution of 4 cm^{-1} and a baseline correction.

Thermal stability

To evaluate the thermal stability of the pristine CNF film and the modified CNF film, thermal gravimetric analysis (TGA, STA 449F5, NETZSCH, Germany) was applied. Sample (approximately 5 mg) was heated from RT to 800 °C at a heating rate of 10 °C/min in nitrogen atmosphere.

Mechanical properties

The mechanical properties of the pristine CNF film and the modified CNF film were analyzed by an electronic universal material testing machine with Bluehill software (LS1, AMETEK, USA). The stretch speed was 1 mm/min, and the load transducer was 50 N. The test distance was 30 mm, and the CNF films were cut into a size of 60 mm × 10 mm. Each sample was measured for three times.

Wettability

The wettability of the pristine CNF film and the modified CNF film was measured by static contact angle instrument (DSA 100, KRUSS, Germany) at RT by a sessile-drop method with 4 μL droplets of deionized water, and images were taken after stabilization for 15 s. Three parallel measurements were carried out for each sample.

Water uptake

The water uptake of the pristine CNF film and the modified CNF film was determined by immersing a strip with a size of 33 mm × 10 mm into an excess amount of deionized water at RT and recording the sample weight after 0.5, 1, 2 and 8 h using a top pan balance. Note that, before weighing, the excess of water should be removed from the sample by a standard roller using blotting papers on both sides of the film. Finally, the water uptake was calculated according to the following equation:

$$Water\ uptake = \frac{m_2 - m_1}{m_1} \times 100 \quad (3)$$

here, m_1 is the weight of the film before immersion, and m_2 is the weight of the film after immersion.

Water vapor permeability (WVP)

The WVP property of the pristine CNF film and the modified CNF film was first investigated by the measurement of their corresponding water vapor transfer rate (WVTR). The WVTR was measured by a water vapor transfer rate testing instrument (TSY-T1, Labthink, China). In brief, the film was cut into a size of 50 mm × 50 mm and put onto a permeability cup previously filled with distilled water (10 mL, RH 100%). The cup was then sealed with a final testing area of 16 cm^2 and put into the dry chamber of the instrument at 38.0 ± 0.6 °C under 10% RH. The sealed cup was weighed periodically (0.001 g) until the testing was completed. Water vapor transporting

into the dry chamber was determined by the weight loss of the cup, and the WVTR value was calculated as the mass of water vapor passing through the film per unit area and time under defined conditions. Three parallel measurements were performed for each sample. In order to eliminate the effect of film thickness, the WVP value was finally calculated by the following equation (Bedane et al. 2015):

$$WVP = \frac{WVTR \times Z \times 100}{P^{sat} \times RH(\%)} = \frac{mass\ H_2O\ lost}{time \times area} \times \frac{Z \times 100}{P^{sat} \times RH(\%)} \quad (4)$$

here, Z is the film thickness, P^{sat} is the water vapor saturation pressure at the experimental temperature, and RH (%) is the percentage relative humidity gradient.

Results and discussion

Morphology of the modified CNFs

The morphology as well as the size distributions of the pristine CNFs and the modified CNFs is shown in Fig. 2. The pristine CNFs (Fig. 2a, c) showed fibrillar shape with a diameter mostly in the range of 30–60 nm and a length of micrometers. In order to insert hydrophobic moieties to the CNFs for barrier application, 10-undecylenoyl chloride was attached to the fibrils by acylation. According to the result of elemental analysis, the calculated DS by Eq. 1 was 0.19. After modification, the diameter of the resulting CNFs (Fig. 2b, d) mainly became thicker with a concentrated range of 70–80 nm. Furthermore, their TEM image (Fig. 2b) displayed that the surface of the modified CNFs turned rougher, which was consistent with the study by Jonoobi (2010). According to their research, this phenomenon could be explained by the fact that the swelling effect of the added pyridine catalyst during the modification favored the penetration of acyl chloride into the swelled fibers and therefore ruptured the cell wall structure. This rough structure of the modified CNFs would affect the properties of the generated CNF films.

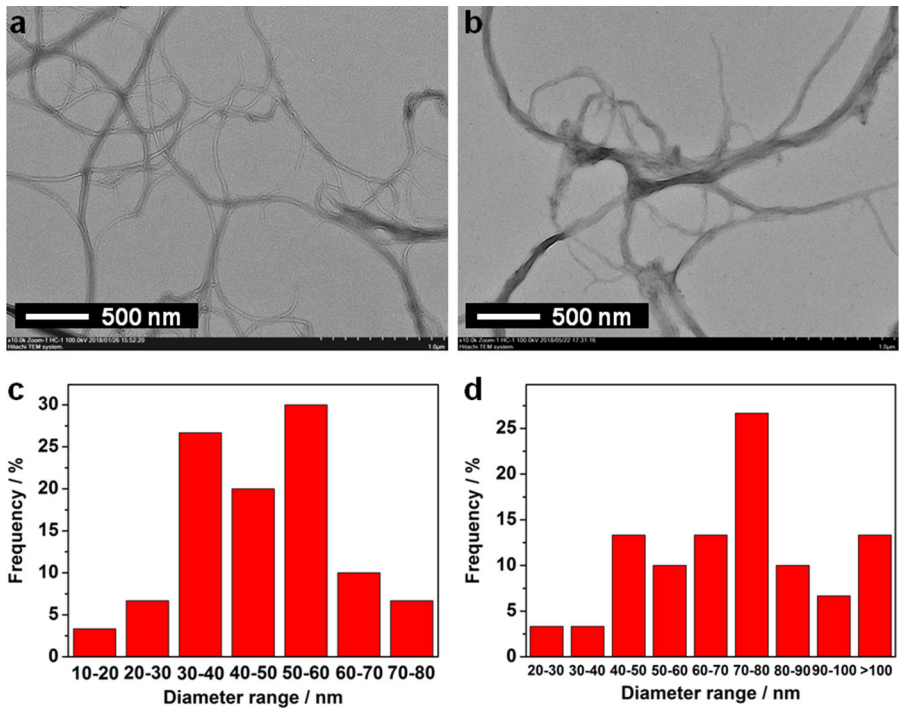

Fig. 2 TEM images and size distributions of the pristine CNFs (**a**, **c**) and the modified CNFs (**b**, **d**)

Dispersion properties of the modified CNFs in solvents and the homogeneity as well as the physical properties of the resulting CNF films.

Since the dispersion solvent plays a key role in the film-forming properties, the dispersion properties of the modified CNFs in different solvents, including water, a mixture of ethanol and water with a volume ratio of 1 to 1, and ethanol, were investigated. The choosing of ethanol here is due to its "low toxicity" and "low boiling temperature". The dispersion images of the modified CNFs in the chosen solvents are provided in Fig. 3a. It could be observed that the CNFs were floated on the surface of water. When they were dispersed in a mixture of ethanol and water, the CNFs were suspended in solution with several fluffy precipitate. However, the modified CNFs homogeneously dispersed in ethanol. This phenomenon could be due to the compatibility of the tethered long alkylene chains in CNFs with organic solvent (Hu et al. 2017), indicating the hydrophobicity of the generated CNFs. In the following, the modified CNFs dispersing in the above three solvents were vacuum filtrated to generate CNF films and the corresponding images of the resulting films are displayed in Fig. 3b. As seen from the images, the film prepared from an ethanol suspension exhibited the most homogenous appearance in comparison to that from the other two suspensions. The obvious white dots in the two films could be the fibril aggregates that resulted from the poor dispersion performance of the modified CNFs in these solvents. Thereby, we could conclude that the best dispersion solvent for the modified CNFs here was ethanol, which was consistent with the result reported by Jonoobi et al. (2010), and the generated CNF film was applied for further investigation. Furthermore, the physical properties of the pristine CNF film and the modified CNF film, including grammage, thickness, density and porosity, are summarized in Table 1. Both of the films had a similar grammage, which matched our preparation method. The thickness of the modified CNF film was (30 ± 1) μm, which was higher than that of the pristine CNF film. This phenomenon could be explained by the fact that the hydrogen bonds between cellulose fibers reduced after modification, which would result in a loose structure of the formed film. In this case, the modified CNF film displayed a lower density in comparison to the pristine CNF film. Furthermore, the calculated porosity of the pristine CNF film and the modified CNF film was (16.7 ± 1.6)% and (35.3 ± 0.5)%, respectively. The increased porosity could be also due to the decreased hydrogen bonds after acylation of CNFs that further leaded to a loose structure of our formed CNF film.

Chemical structure of the modified CNF film

The chemical structure of the modified CNF film was identified by FTIR spectroscopy, and the corresponding spectra with magnification at defined regions in a comparison to the pristine CNF film are given in Fig. 4. After acylation, a new band appeared at 1732 cm^{-1}, which was the characteristic stretching vibration of carboxyl groups (Tomé et al. 2011). Meanwhile, the signals of methylene groups as well as methyl groups at 2854, 2915 and 557 cm^{-1} became stronger (Nair et al. 2017). Additionally, there was a weak band at 3077 cm^{-1} in the modified CNF film, which could be the stretching vibration of the attached –CH=CH_2 groups. The blue shift at 1625 and 903 cm^{-1} could be attributed to the stretching vibration of C=C groups and deformation vibration of alkene C–H groups, respectively (Wang et al. 2016). The low intensity of the FTIR signals of alkene also suggested the low DS of acylation, which was consistent with the calculated small DS value (0.19). All these results indicated the successful attachment of

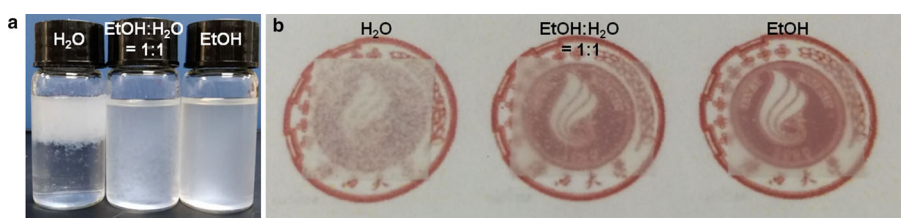

Fig. 3 **a** Dispersion images of the modified CNFs in different solvents; and **b** images of the modified CNF films prepared from different solvents (from left to right: water, a mixture of ethanol and water with a volume ratio of 1 to 1, ethanol)

Table 1 Physical properties, including grammage, thickness, density and porosity, of the pristine CNF film (CNF film-1) and the modified CNF film (CNF film-2)

Sample	Grammage (g m^{-2})	Thickness (μm)	Density (g cm^{-3})	Porosity (%)
CNF film-1	30 ± 1	24 ± 1	1.25 ± 0.03	16.7 ± 1.6
CNF film-2	29 ± 1	30 ± 1	0.97 ± 0.01	35.3 ± 0.5

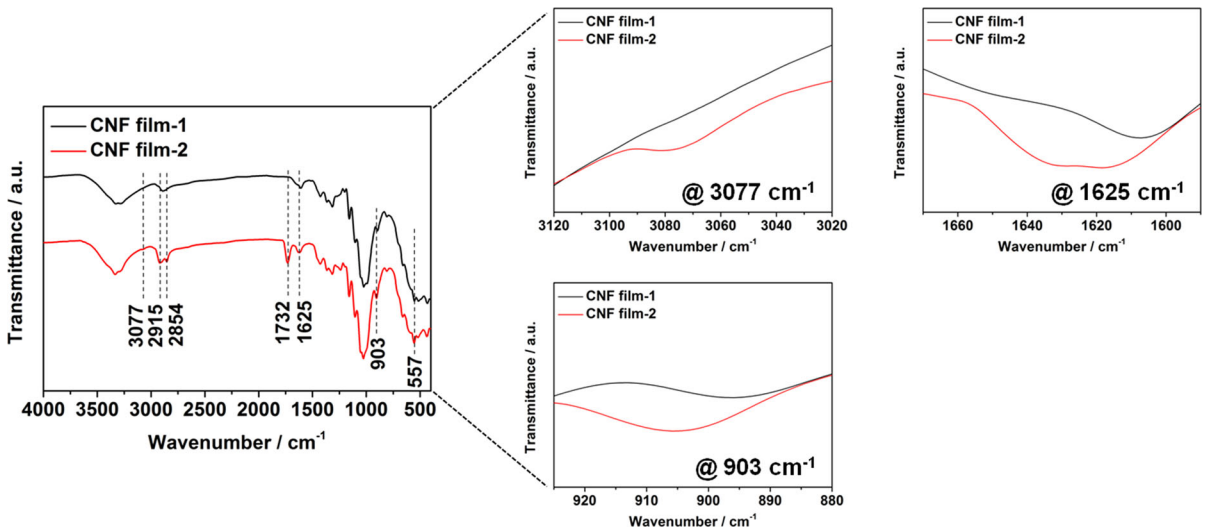

Fig. 4 FTIR spectra of the pristine CNF film (CNF film-1) and the modified CNF film (CNF film-2) with magnification at defined regions

10-undecylenoyl chloride onto the CNFs. Furthermore, the appearance of C=C groups on the film surface would provide further reactive properties of the resulting CNF film, for example, by photoinduced thiol-ene click reaction for additional functionalization (Guo et al. 2016; Li et al. 2014), to broaden their packaging applications.

Morphology of the modified CNF film

The surface morphology of the modified CNF film was investigated by SEM and AFM with the pristine CNF film used as reference. As seen from their SEM images (Fig. 5a, f), both of the films showed obvious interconnected fibrous networks with large aggregates-bundles of fibrils. Meanwhile, there were more aggregates on the surface of the modified CNF film, which could be due to the film preparation method, that is, during solvent drainage and network formation, the modified CNFs with hydrophobic groups were forced out of the film networks. This phenomenon was also observed in Andresen's research (2006). Furthermore, since the concentration of the modified CNF suspension for the film preparation was higher than that in the above dispersibility study, the modified CNFs would be aggregated during film formation by the hydrophobic interaction. Furthermore, we could observe a homogeneous surface of the modified CNF film from its SEM cross-section image (Fig. 5g), indicating the grafting homogeneity of our film. Additionally, a rougher surface could be seen from Fig. 5g in comparison to that of the pristine CNF film (Fig. 5b). With further investigation by AFM (Fig. 5c–e and h–j), we could observe that both of the films well dispersed. After modification, thick fibers appeared with large aggregates, which was consistent with their TEM and SEM images. The calculated roughness of the pristine CNF film and the modified CNF film was 6.069 and 8.763, respectively. The increased surface roughness of the modified CNF film could be due to the rough structure of the modified CNFs as shown in the TEM image, which would

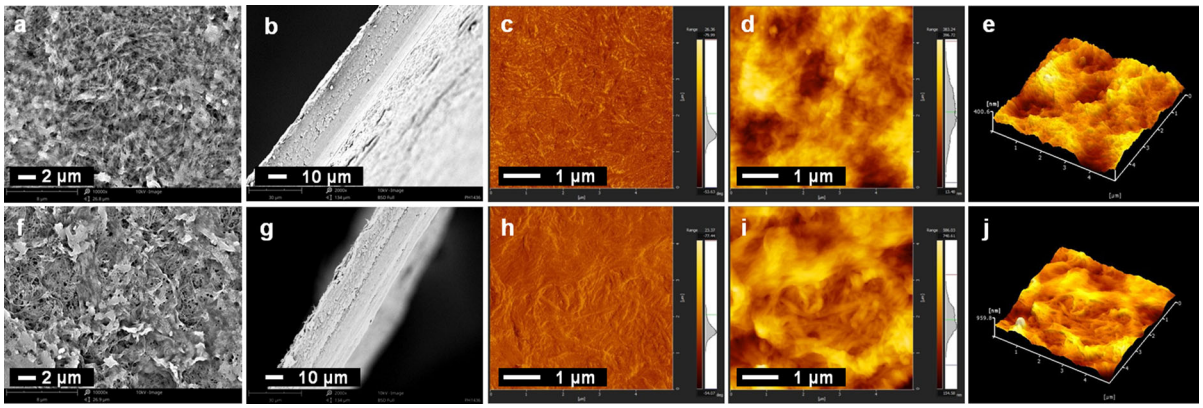

Fig. 5 SEM surface images (**a**, **f**), cross-section images (**b**, **g**) and AFM images (**c**, **d**, **e**, **h**, **i**, **j**) of the pristine CNF film (top) and the modified CNF film (down)

further decrease the surface wettability of the modified CNF film.

Thermal stability of the modified CNF film

The impact of acylation on the thermal stability of the generated CNF film was investigated by TGA. Figure 6a demonstrates the TGA curves of the modified CNF film and the pristine CNF film. The pristine CNF film showed a weight loss before 200 °C, which could be resulted from the free and bound water in the CNF film due to the hygroscopicity of the cellulose fibers. However, the modified CNF film exhibited a less weight loss in the same temperature region, indicating the hydrophobicity of the resulting CNF film. Furthermore, a sharp weight loss appeared at 343 and 350 °C for the pristine CNF film and the modified CNF film, respectively, which was consistent with the exothermic peak in their corresponding DTG curves (Fig. 6b). The weight loss here could be attributed to the decomposition of the cellulose structure (Abraham et al. 2011). This phenomenon indicated that a slight enhancement of the thermal stability was obtained after acylation, which was consistent with the literature (Tingaut et al. 2010). Furthermore, according to the literatures (Peng et al. 2013; Zhang et al. 2018), the final residue for NFC sample at a temperature of 600 °C was char. Meanwhile, Yang et al. (2006) reported a total of ∼ 67 wt% of lignin was lost at 850 °C. Thereby, the residual component in our system was char and part lignin. Since the pristine as well as the modified CNF films had a similar grammage, the lower residual mass in the modified film could be due to its lower content of the CNFs in comparison to that of the pristine film. This result also suggested the successful attachment of the aliphatic chains onto the CNFs.

Mechanical properties of the modified CNF film

As for packaging application, the mechanical properties are of great importance to know. Thereby, the tensile strength, elongation at break and tensile modulus of the pristine as well as the modified CNF

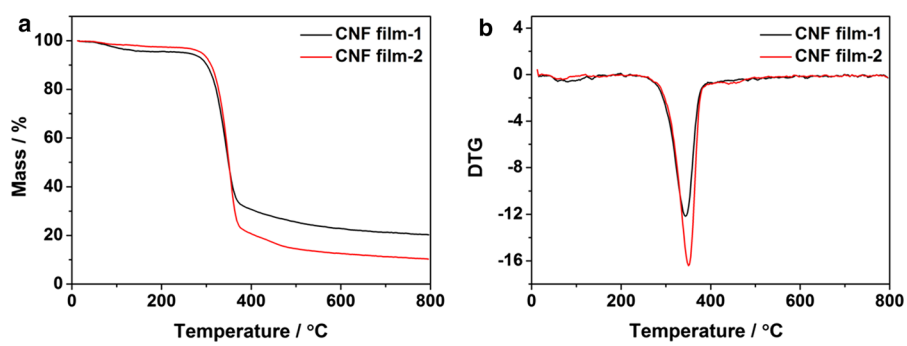

Fig. 6 TGA (**a**) and DTG (**b**) curves of the pristine CNF film (CNF film-1) and the modified CNF film (CNF film-2)

films were measured and the result is provided in Fig. 7. The pristine CNF film showed a tensile strength of (57 ± 2) MPa, elongation at break of (4.5 ± 0.8)% and tensile modulus of (3847 ± 150) MPa, which could be resulted from the strong hydrogen bonds among the entangled nanofibers. After modification of the CNFs, the resulting CNF film exhibited a decrease in tensile strength [(47 ± 4) MPa], an increase in elongation at break [(6.2 ± 0.9)%], and a decrease in tensile modulus [(2075 ± 180) MPa]. This phenomenon could be explained by the fact that the attached molecular chains reduced the hydrogen bonds. Even so, the modified CNF film still had a high tensile stress, which could be advantageous to its packaging application.

Wettability, water uptake and barrier property of the modified CNF film

The contact angle images of the pristine CNF film and the modified CNF film captured after 15 s are displayed in Fig. 8a. Interestingly, the pristine CNF film had a water contact angle of (54 ± 2)°. This phenomenon was also observed by other researchers (Ferrer et al. 2012; Rojo et al. 2015; Spence et al. 2010). Spence et al. (2010) reported the initial contact angle of homogenized samples from different wood sources ranged from (48.2 ± 9.4)° to (88.1 ± 9.4)°, and they addressed that lignin as hydrophobic polymer in nanofibers was contributed to the high water contact angle. Specifically, lignin decreases the surface energy of the fibrils, which can be expected from the larger percentage of C–C and C–H bonds as well as the lower O/C ratio in comparison to cellulose (Rojo et al. 2015; Laine and Stenius 1994). In Qing's research (Qing et al. 2015), the water contact angle of neat CNF film was 65.1° after holding 120 s. They explained this result by the surface roughness of the CNF film, leading to the formation of air pockets between the rough surface and the droplet. Since the applied pulp here for CNF production had a lignin content of 5.2% (Nie et al. 2018) and the pristine CNF film displayed surface roughness as shown in the AFM result, we could conclude that the above-mentioned two factors were attributed to the high contact angle of the pristine CNF film in our research. After the attachment of 10-undecylenoyl chloride onto the CNFs, the resulting film showed a contact angle of approximately (101 ± 2)°, indicating the hydrophobic performance of the modified CNF film, which could be due to the low surface energy from the attached nonpolar long aliphatic chains.

Figure 8b illustrates the water uptake (wt%) of the pristine and the modified CNF films calculated by Eq. 3. The maximum water uptake rate of the pristine CNF film occurred in the first 0.5 h, which was due to the very hygroscopic character of the cellulose fibers. Thereafter, the rate decreased, and the water uptake almost reached a saturation level after immersion for 2 h with a value of approximately 95%, which was consistent with the literature (Nair et al. 2017). However, the modified CNF film showed a weak water uptake behavior. The water uptake leveled off at just about 6% after an immersion time of 0.5 h, suggesting the hydrophobicity of the generated CNF film.

In the following, the barrier property of the modified CNF film was described by water vapor permeability (WVP). According to Eq. 4, the calculated WVP values of the pristine CNF film and the modified CNF film were (9.022 ± 0.18) × 10^{-9} and (3.396 ± 0.09) × 10^{-9} g m^{-1} s^{-1} Pa^{-1}, respectively, as shown in Fig. 8c. This result suggested that after the hydrophobic modification, the WVP value of the

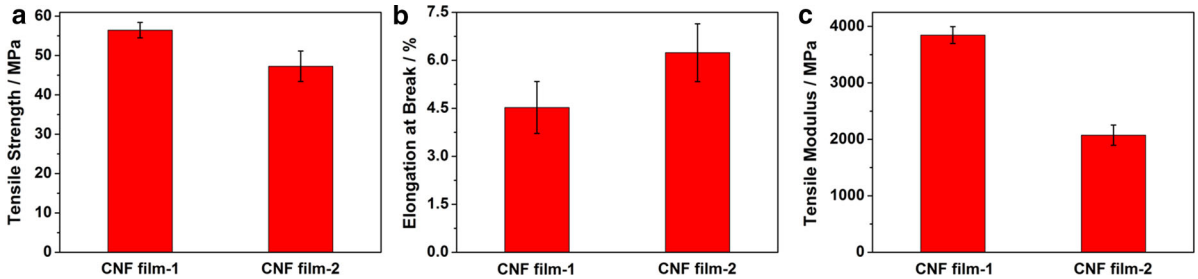

Fig. 7 Tensile stress (**a**), elongation at break (**b**) and tensile modulus (**c**) of the pristine CNF film (CNF film-1) and the modified CNF film (CNF film-2)

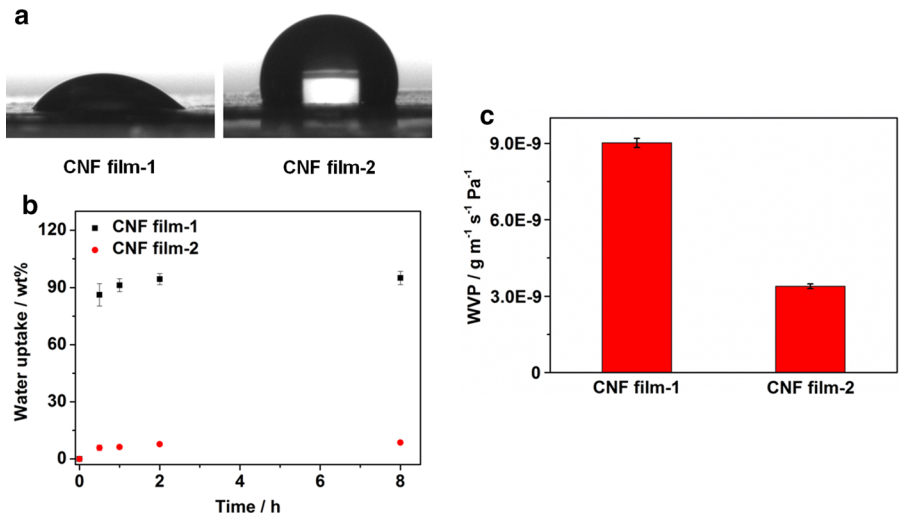

Fig. 8 **a** Contact angle images of the pristine CNF film (CNF film-1) and the modified CNF film (CNF film-2); **b** water uptake of the pristine CNF film (CNF film-1) and the modified CNF film (CNF film-2); and **c** WVP of the pristine CNF film (CNF film-1) and the modified CNF film (CNF film-2)

generated CNF film decreased by about 62.4%, which showed an obvious improvement of the vapor barrier property of the modified CNF film compared with the results reported by Solala et al. (2018) who addressed water vapor transport was not influenced by the surface hydrophobization. This phenomenon can be explained by the following two factors: (1) the higher contact angle of our formed film produced by first hydrophobization of the CNFs followed by vacuum filtration [(101 ± 2)° for our film and approximately 55° for Solala's film]; (2) the lower porosity of our formed film prepared without solvent exchange after film formation [(35.3 ± 0.5)% for our film and (45 ± 8)% for Solala's film].

Reactivity of the modified CNF film

As is known to us, the C=C groups can undergo photoinduced thiol-ene click reaction. Therefore, in order to check the reactivity of the modified CNF film, the film was reacted with 3-mercaptopropionic acid under UV illumination. The corresponding procedure is illustrated in Fig. 9a. The FTIR spectra of the reacted CNF film in comparison to the modified CNF film are displayed in Fig. 9b. The weak band at 3077 cm^{-1} in the modified CNF film that was ascribed to the stretching vibration of the attached –CH=CH_2 groups disappeared, indicating the reaction of thiol groups with C=C groups. Moreover, as for the reacted CNF film, the obvious red shift at 1732 cm^{-1} suggested the appearance of the carboxylic groups. The further blue shift at 1625 cm^{-1} might be due to the absorbed water by the attached carboxylic groups (Wang et al. 2016). However, it was difficult to find out the signal of C–S–C groups, which could be overlapped with that of C–O–C groups from CNFs themselves. Additionally, Fig. 9c illustrates the SEM image of the reacted CNF film. It could be seen that the film still exhibited fibrous structure with part aggregates, which was similar to the morphology of the modified CNF film before reaction (Fig. 5e). This phenomenon suggested the photoinduced thiol-ene reaction was facile, which would be beneficial to the further application. Finally, the wettability of the reacted CNF film was checked by contact angle measurement. As shown in Fig. 9d, after reaction, the contact angle of the modified CNF film changed from (101 ± 2)° to (71 ± 1)°, which was still higher than that of the pristine CNF film [(54 ± 2)°], indicating the successful attachment of the hydrophilic carboxylic groups by photoreaction. This phenomenon also indicated the reactivity of the modified CNF film, which showed the possibility of further functionalization to enrich the properties of the generated CNF film.

Conclusions

In summary, reactive hydrophobic CNF film was successfully prepared by a facile strategy with the attachment of 10-undecylenoyl chloride onto CNFs followed by vacuum filtration. The modified CNFs became thicker and rougher and were easy to disperse in ethanol. The generated CNF film showed obvious

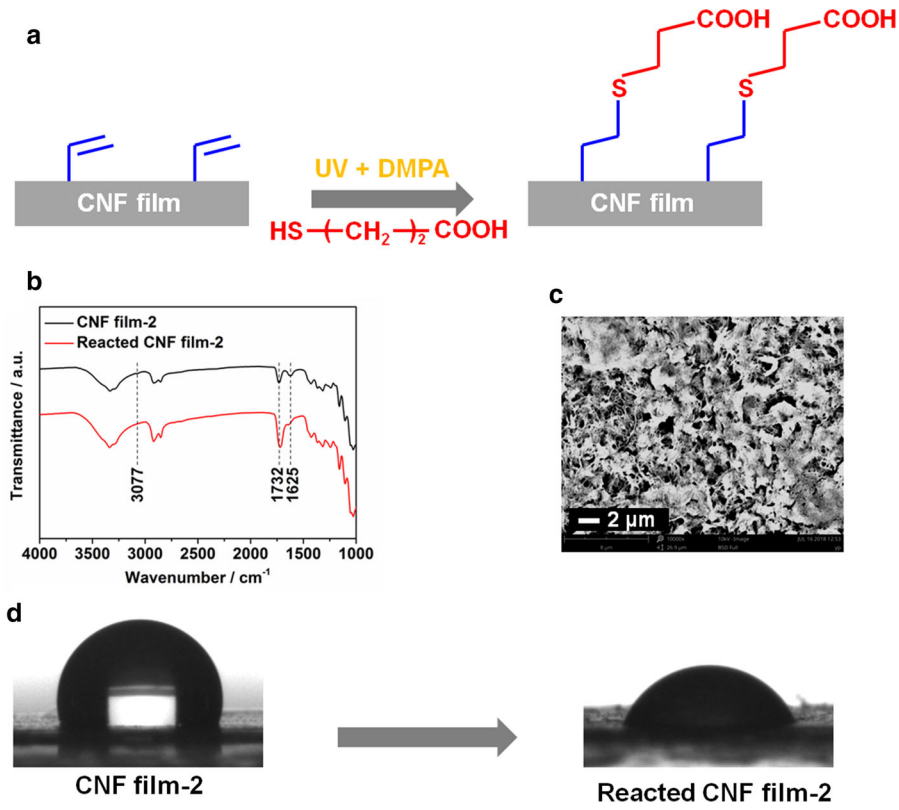

Fig. 9 **a** Schematic illustration of the reactivity of the modified CNF film; **b** FTIR spectra of the modified CNF film (CNF film-2) and the reacted CNF film (reacted CNF film-2); **c** SEM image of the reacted CNF film; and **d** contact angle images of the modified CNF film (CNF film-2) and the reacted CNF film (reacted CNF film-2)

interconnected fibrous networks with more large aggregates-bundles of fibrils and increased surface roughness compared with the pristine CNF film. The modified CNF film also exhibited a slightly better thermal stability. Although the modification reduced the hydrogen bonds among fibers, the resulting CNF film still showed a high tensile strength of (47 ± 4) MPa. Furthermore, the formed CNF film was hydrophobic and showed an obvious barrier improvement with the WVP value decreasing by 62.4% in comparison to the pristine CNF film. Since this hydrophobic CNF film is easy to prepare and is a good vapor barrier, it is a good candidate for packaging applications. Additionally, the reactivity of the C=C groups on its surface can be further functionalized to enrich their applications.

Acknowledgments This work was supported by the Natural Science Foundation of Guangxi (2018GXNSFBA138027), Scientific Research Foundation of Guangxi University (XGZ170232), the State Key Laboratory of Pulp and Paper Engineering (201806), the Foundation of Key Laboratory of Pulp and Paper Science and Technology of Ministry of Education/Shandong Province of China (KF201716) and the Middle-young Age Ability Enhancement Program of Guangxi (2018KY0023).

Compliance with ethical standards

Conflict of interest The authors declare that they have no conflict of interest.

References

Abdul Khalil HPS, Davoudpour Y, Islam MN, Mustapha A, Sudesh K, Dunqani R, Jawaid M (2014) Production and modification of nanofibrillated cellulose using various mechanical processes: a review. Carbohydr Polym 99:649–665. https://doi.org/10.1016/j.carbpol.2013.08.069

Abraham E, Deepa B, Pothan LA, Jacob M, Thomas S, Cvelbar U, Anandjiwala R (2011) Extraction of nanocellulose fibrils from lignocellulosic fibers: a novel approach. Carbohydr Polym 86:1468–1475. https://doi.org/10.1016/j.carbpol.2011.06.034

Andresen M, Johansson LS, Tanem BS, Stenius P (2006) Properties and characterization of hydrophobized microfibrillated cellulose. Cellulose 13:665–677. https://doi.org/10.1007/s10570-006-9072-1

Aulin C, Gällstedt M, Lindström T (2010) Oxygen and oil barrier properties of microfibrillated cellulose films and

coatings. Cellulose 17:559–574. https://doi.org/10.1007/s10570-009-9393-y

Azeredo HMC, Rosa MF, Mattoso LHC (2017) Nanocellulose in bio-based food packaging applications. Ind Crops Prod 97:664–671. https://doi.org/10.1016/j.indcrop.2016.03.013

Bedane AH, Eić M, Farmahini-Farahani M, Xiao H (2015) Water vapor transport properties of regenerated cellulose and nanofibrillated cellulose films. J Membr Sci 493:46–57. https://doi.org/10.1016/j.memsci.2015.06.009

Benitez AJ, Torres-Rendon JG, Poutanen M, Walther A (2013) Humidity and multiscale structure govern mechanical properties and deformation modes in films of native cellulose nanofibrils. Biomacromolecules 14:4497–4506. https://doi.org/10.1021/bm401451m

Chinga-Carrasco G, Kuznetsova N, Garaeva M, Leirset I, Galiullina G, Kostochko A, Syverud K (2012) Bleached and unbleached MFC nanobarriers: properties and hydrophobisation with hexamethyldisilazane. J Nanopart Res 14:1280. https://doi.org/10.1007/s11051-012-1280-z

Cunha AG, Zhou Q, Larsson PT, Berglund LA (2014) Topochemical acetylation of cellulose nanopaper structures for biocomposites: mechanisms for reduced water vapour sorption. Cellulose 21:2773–2787. https://doi.org/10.1007/s10570-014-0334-z

Ferrer A, Quintana E, Filpponen I, Solala I, Vidal T, Rodríguez A, Laine J, Rojas OJ (2012) Effect of residual lignin and heteropolysaccharides in nanofibrillar cellulose and nanopaper from wood fibers. Cellulose 19:2179–2193. https://doi.org/10.1007/s10570-012-9788-z

Ferrer A, Pal L, Hubbe M (2017) Nanocellulose in packaging: advances in barrier layer technologies. Ind Crops Prod 95:574–582. https://doi.org/10.1016/j.indcrop.2016.11.012

Guo J, Fang W, Welle A, Feng W, Filpponen I, Rojas OJ, Levkin PA (2016) Superhydrophobic and slippery lubricant-infused flexible transparent nanocellulose films by photoinduced thiol-ene functionalization. ACS Appl Mater Interfaces 8:34115–34122. https://doi.org/10.1021/acsami.6b11741

Hu Z, Berry RM, Pelton R, Cranston ED (2017) One-pot water-based hydrophobic surface modification of cellulose nanocrystals using plant polyphenols. ACS Sustain Chem Eng 5:5018–5026. https://doi.org/10.1021/acssuschemeng.7b00415

Johnson RK, Zink-Sharp A, Glasser WG (2011) Preparation and characterization of hydrophobic derivatives of TEMPO-oxidized nanocelluloses. Cellulose 18:1599–1609. https://doi.org/10.1007/s10570-011-9579-y

Jonoobi M, Harum J, Mathew AP, Hussein MZB, Oksman K (2010) Preparation of cellulose nanofibers with hydrophobic surface characteristics. Cellulose 17:299–307. https://doi.org/10.1007/s10570-009-9387-9

Klemm D, Philipp B, Heinze T, Heinze U, Wagenknecht W (1998) Comprehensive cellulose chemistry: functionalization of cellulose. Wiley-VCH, Weinheim

Laine J, Stenius P (1994) Surface characterization of unbleached kraft pulps by means of ESCA. Cellulose 1:145–160. https://doi.org/10.1007/BF00819664

Le D, Kongparakul S, Samart C, Phanthong P, Karnjanakom S, Abudula A, Guan G (2016) Preparation hydrophobic nanocellulose-silica film by a facile one-pot method. Carbohydr Polym 153:266–274. https://doi.org/10.1016/j.carbpol.2016.07.112

Li J, Li L, Du X, Feng W, Welle A, Trapp O, Grunze M, Hirtz M, Levkin PA (2014) Reactive superhydrophobic surface and its photoinduced disulfide-ene and thiol-ene (bio)functionalization. Nano Lett 15:675–681. https://doi.org/10.1021/nl5041836

Lu P, Tian X, Liu Y, Wang Z (2016) Effects of Cellulosic based sheet pore structure and soybean oil-based polymer layer on cellulosic packaging performance as a barrier for water and water vapor. BioRes. 11:8483–8495. https://doi.org/10.15376/biores.11.4.8483-8495

Nair SS, Yan N (2015) Effect of high residual lignin on the thermal stability of nanofibrils and its enhanced mechanical performance in aqueous environments. Cellulose 22:3137–3150. https://doi.org/10.1007/s10570-015-0737-5

Nair SS, Kuo PY, Chen H, Yan N (2017) Investigating the effect of lignin on the mechanical, thermal, and barrier properties of cellulose nanofibril reinforced epoxy composite. Ind Crops Prod 100:208–217. https://doi.org/10.1016/j.indcrop.2017.02.032

Nechyporchuk O, Belgacem MN, Bras J (2016) Production of cellulose nanofibrils: a review of recent advances. Ind Crops Prod 93:2–25. https://doi.org/10.1016/j.indcrop.2016.02.016

Nie S, Zhang K, Lin X, Zhang C, Yan D, Liang H, Wang S (2018) Enzymatic pretreatment for the improvement of dispersion and film properties of cellulose nanofibrils. Carbohydr Polym 181:1136–1142. https://doi.org/10.1016/j.carbpol.2017.11.020

Österberg M, Vartiainen J, Lucenius J, Hippi U, Seppälä J, Serimaa R, Laine J (2013) A fast method to produce strong NFC films as a platform for barrier and functional materials. ACS Appl Mater Interfaces 5:4640–4647. https://doi.org/10.1021/am401046x

Peng Y, Gardner DJ, Han Y, Kiziltas A, Cai Z, Tshabalala MA (2013) Influence of drying method on the material properties of nanocellulose I: thermostability and crystallinity. Cellulose 20:2379–2392. https://doi.org/10.1007/s10570-013-0019-z

Poletto M, Zarrera AJ, Forte MMC, Santana RMC (2012) Thermal decomposition of wood: influence of wood components and cellulose crystallite size. Bioresour Technol 109:148–153. https://doi.org/10.1016/j.biortech.2011.11.122

Prakobna K, Terenzi C, Zhou Q, Furó I, Berglund LA (2015) Core-shell cellulose nanofibers for biocomposite-nanostructural effects in hydrated state. Carbohydr Polym 125:92–102. https://doi.org/10.1016/j.carbpol.2015.02.059

Qing Y, Cai Z, Wu Y, Yao C, Wu Q, Li X (2015) Facile preparation of optically transparent and hydrophobic cellulose nanofibril composite films. Ind Crops Prod 77:13–20. https://doi.org/10.1016/j.indcrop.2015.08.016

Rajinipriya M, Nagalakshmaiah M, Robert M, Elkoun S (2018) Importance of agricultural and industrial waste in the field of nanocellulose and recent industrial developments of wood based nanocellulose: a review. ACS Sustain Chem

Eng 6:2807–2828. https://doi.org/10.1021/acssuschemeng.7b03437

Rojo E, Peresin MS, Sampson WW, Hoeger IC, Vartiainen J, Laine J, Rojas OJ (2015) Comprehensive elucidation of the effect of residual lignin on the physical, barrier, mechanical and surface properties of nanocellulose films. Green Chem 17:1853–1866. https://doi.org/10.1039/C4GC02398F

Sehaqui H, Zimmermann T, Tingaut P (2014) Hydrophobic cellulose nanopaper through a mild esterification procedure. Cellulose 21:367–382. https://doi.org/10.1007/s10570-013-0110-5

Shimizu M, Saito T, Fukuzumi H, Isogai A (2014) Hydrophobic, ductile, and transparent nanocellulose films with quaternary alkylammonium carboxylates on nanofibril surfaces. Biomacromol 15:4320–4325. https://doi.org/10.1021/bm501329v

Shimizu M, Saito T, Isogai A (2016) Water-resistant and high oxygen-barrier nanocellulose films with interfibrillar cross-linkages formed through multivalent metal ions. J Membr Sci 500:1–7. https://doi.org/10.1016/j.memsci.2015.11.002

Solala I, Bordes R, Larsson A (2018) Water vapor mass transport across nanofibrillated cellulose films: effect of surface hydrophobization. Cellulose 25:347–356. https://doi.org/10.1007/s10570-017-1608-z

Song J, Rojas OJ (2013) Approaching super-hydrophobicity from cellulosic materials: a review. Nord Pulp Pap Res J 28:216–238

Song Z, Xiao H, Zhao Y (2014) Hydrophobic-modified nano-cellulose fiber/PLA biodegradable composites for lowering water vapor transmission rate (WVTR) of paper. Carbohydr Polym 111:442–448. https://doi.org/10.1016/j.carbpol.2014.04.049

Spence KL, Venditti RA, Rojas OJ, Habibi Y, Pawlak JJ (2010) The effect of chemical composition on microfibrillar cellulose films from wood pulps: water interactions and physical properties for packaging applications. Cellulose 17:835–848. https://doi.org/10.1007/s10570-010-9424-8

Stenstad P, Andresen M, Tanem BS, Stenius P (2008) Chemical surface modifications of microfibrillated cellulose. Cellulose 15:35–45. https://doi.org/10.1007/s10570-007-9143-y

Teisala H, Tuominen M, Kuusipalo J (2014) Superhydrophobic coatings on cellulose-based materials: fabrication, properties, and applications. Adv Mater Interfaces 1:1300026. https://doi.org/10.1002/admi.201300026

Tingaut P, Zimmermann T, Lopez-Suevos F (2010) Synthesis and characterization of bionanocomposites with tunable properties from poly(lactic acid) and acetylated microfibrillated cellulose. Biomacromol 11:454–464. https://doi.org/10.1021/bm901186u

Tomé LC, Pinto RJB, Trovatti E, Freire CSR, Silvestre AJD, Neto CP, Gandini A (2011) Transparent bionanocomposties with improved properties prepared from acetylated bacterial cellulose and poly(lactic acid) through a simple approach. Green Chem 13:419–427. https://doi.org/10.1039/C0GC00545B

Vaca-Garcia C, Borredon ME, Gaseta A (2001) Determination of the degree of substitution (DS) of mixed cellulose esters by elemental analysis. Cellulose 8:225–231. https://doi.org/10.1023/A:1013133921626

Wang Y, Heinze T, Zhang K (2016) Stimuli-responsive nanoparticles from ionic cellulose derivatives. Nanoscale 8:648–657. https://doi.org/10.1039/c5nr05862g

Wang J, Gardner DJ, Stark NM, Bousfield DW, Tajvidi M, Cai Z (2018a) Moisture and oxygen barrier properties of cellulose nanomaterial-based films. ACS Sustain Chem Eng 6:49–70. https://doi.org/10.1021/acssuschemeng.7b03523

Wang S, Sha J, Wang W, Qin C, Li W, Qin C (2018b) Superhydrophobic surfaces generated by one-pot spray-coating of chitosan-based nanoparticles. Carbohydr Polym 195:39–44. https://doi.org/10.1016/j.carbpol.2018.04.068

Yang H, Yan R, Chen H, Zheng C, Lee DH, Liang DT (2006) In-depth investigation of biomass pyrolysis based on three major components: hemicelluloses, cellulose and lignin. Energy Fuels 20:388–393. https://doi.org/10.1021/ef0580117

Zhang K, Zhang Y, Yan D, Zhang C, Nie S (2018) Enzyme-assisted mechanical production of cellulose nanofibrils: thermal stability. Cellulose. https://doi.org/10.1007/s10570-018-1928-7